Cover Letter

INTEGRATE - a Python package for fast localized probabilistic inversion using informed priors, applied to EM data

Thomas Mejer Hansen,Frederik Alexander Falk,Flemming Jørgensen,Jesper Nørgaard

This is as a non-peer reviewed preprint submitted to EarthArXiv, that is currently under review in Computers and Geosciences.

Highlights

INTEGRATE - a Python package for fast localized probabilistic inversion using informed priors, applied to EM data

Thomas Mejer Hansen,Frederik Alexander Falk,Flemming Jørgensen,Jesper Nørgaard

- Efficient probabilistic inversion using rejection sampling with temperature annealing.
- Inclusion of arbitrarily complex prior information.
- Multi-modal framework simultaneously inverts electromagnetic and well-log data.
- Parallel processing handles millions of realizations with optimized memory usage.
- `HDF5`-based workflow integrates GA-AEM forward modeling for practical applications.

INTEGRATE - a Python package for fast localized probabilistic inversion using informed priors, applied to EM data

Thomas Mejer Hansen[a], Frederik Alexander Falk[a], Flemming Jørgensen[c] and Jesper Nørgaard[b]

[a]Department of Geoscience, Aarhus University, Høegh-Guldbergs Gade 2, 8000 Aarhus C, Denmark
[b]Near-surface Land and Marine Geology, Geological Survey of Denmark and Greenland (GEUS), Aarhus, Denmark
[c]Region of Central Denmark, Skottenborg, 8800 Viborg, Denmark

ARTICLE INFO

Keywords:
Probabilistic inversion
electromagnetic geophysics
probabilistic data integration
rejection sampling
uncertainty quantification
geophysical modeling

ABSTRACT

We present INTEGRATE, a Python package for fast localized probabilistic inversion of geophysical data. The framework provides a general approach for Bayesian inference in localized inverse problems, where the same prior information applies to many independent datasets. INTEGRATE implements an extended rejection sampling algorithm with temperature annealing for efficient posterior sampling. The package is modular and open, supporting both continuous and discrete model parameters, arbitrarily complex prior information, flexible noise models (including multivariate Gaussian and multinomial distributions), and parallel processing with shared-memory optimization. All data exchange is handled through `HDF5`, allowing seamless integration with external forward modeling codes and easy adaptation to a wide range of geophysical or non-geophysical applications. We demonstrate the framework for electromagnetic (EM) inversion, integrating time-domain EM using informed geological priors, achieving over 200× speedups relative to traditional MCMC approaches. INTEGRATE efficiently computes Bayesian evidence for hypothesis testing and model comparison. A case study from Daugaard, Denmark (11,693 soundings) illustrates the method's performance, including automatic annealing temperature selection and the influence of lookup-table size on computational efficiency. The open-source package provides command-line tools and visualization utilities, facilitating integration into existing geophysical workflows.

CRediT authorship contribution statement

Thomas Mejer Hansen: Development, Implementation, Writing. **Frederik Alexander Falk:** Development, Writing. **Flemming Jørgensen:** Development, Writing. **Jesper Nørgaard:** Development, Writing.

1. Introduction

Inverse problems in geophysics involve inferring subsurface properties from indirect measurements obtained at or near the Earth's surface. These problems are fundamental to our understanding of subsurface structures and are essential in applications ranging from groundwater exploration to mineral resource assessment. Traditionally, deterministic methods have dominated the field of geophysical inversion (Golub et al., 1999; Menke, 2012). For example, Tikhonov regularization and linearized least squares methods aim to find a single optimal model that fits the observed data within a predefined noise level. These methods are computationally attractive, simple to implement, and can handle relatively large datasets effectively. However, they face two significant limitations. First, it is not trivial to fully characterize the uncertainty associated with the inferred optimal model, which may be just one of many models fitting the data within the noise. This makes uncertainty quantification challenging. Second, deterministic methods typically rely on rather simple prior information, usually based on Gaussian models, making it difficult to incorporate existing knowledge that may be more complex.

The probabilistic approach to inversion allows combining complex prior information and nonlinear data with complex noise characteristics into a posterior probability distribution representing the combined available information (Tarantola and Valette, 1982b; Sambridge, 1999; Tarantola and Valette, 1982a; Tarantola, 2005). Markov chain Monte Carlo (MCMC) sampling methods have been proposed (Mosegaard and Tarantola, 1995; Sambridge and Mosegaard, 2002; Mosegaard and Tarantola, 2002; Amaya et al., 2021) that enable sampling from the posterior distribution. These methods allow generating multiple realizations of subsurface models, representing the combined information in the posterior distribution. Such a set of models captures the full posterior knowledge and uncertainty. This probabilistic framework allows for better quantification of uncertainties and the inclusion of intricate prior knowledge.

Despite the theoretical advantages of probabilistic approaches, MCMC methods have not seen widespread adoption in geophysical inversion due to two fundamental limitations. First, MCMC methods are known to be extremely computationally expensive (Laloy and Vrugt, 2012; Cordua et al., 2012; Hansen et al., 2013), especially for large-scale or high-dimensional problems. This computational burden has limited their practical application in many geophysical contexts even though a lot of work has been done to increase the efficiency using for example Hamiltonian Monte Carlo (HMC) algorithms (Neal et al., 2011; Zunino et al., 2023) that utilizes information about the gradient of the posterior distribution to sample the posterior distribution more effi-

ORCID(s): `0000-0003-4529-0112` (T.M. Hansen);
`https://orcid.org/0009-0003-1023-5161` (F.A. Falk);
`https://orcid.org/0000-0002-2940-5808` (F. Jørgensen);
`https://orcid.org/0000-0002-3317-5101` (J. Nørgaard)

ciently.

Second, while these methods can in principle incorporate complex prior information (Hansen et al., 2008, 2013), they are still computationally expensive (Linde et al., 2015), and when using informed prior models it may not be possible to utilize for example HMC methods, as they rely on being able to compute the gradient of the posterior distribution, which is not always possible for complex prior models.

For specific types of inverse problems, the posterior distribution can be sampled much more efficiently. Localized inverse problems, where the same prior model applies to many independent data sets, can benefit from specialized approaches that exploit this structure to dramatically increase computational efficiency (Hansen, 2021; Spremić et al., 2025).

To address these challenges, we present INTEGRATE, a Python framework for localized probabilistic inversion of geophysical data. The framework implements and extends the localized rejection sampling algorithm (Hansen, 2021) with lookup tables and temperature annealing, providing efficient sampling of the posterior distribution. INTEGRATE is flexible, supporting both continuous and discrete parameters as well as multi modal data integration. It includes built in tools for data handling, model parameterization, and visualization. A key capability is the efficient computation of Bayesian evidence, enabling formal hypothesis testing and model comparison.

Although demonstrated here for the inversion of electromagnetic (EM) data, INTEGRATE is general and applicable to other localized geophysical problems. The open-source package (MIT license) is available at `https://github.com/cultpenguin/integrate_module`.

2. Theory and Methods

2.1. Probabilistic inversion

Consider a set of model parameters $\mathbf{k}$. Such model parameters could refer to resistivity, lithological units, or any other parameters used to describe the subsurface. As an example we split the model parameters into two distinct types, $\mathbf{k} = [\mathbf{m}, \mathbf{n}]$. $\mathbf{m}$ can refer to geophysical continuous model parameters, such as resistivity, and $\mathbf{n}$ can refer to discrete lithological units (Hansen and Minsley, 2019; Hansen, 2021; Madsen et al., 2023).

Two types of information are assumed to be available about the model parameters $[\mathbf{m}, \mathbf{n}]$. The first type of information is *prior information*, quantified through the prior probability distribution $\rho(\mathbf{m}, \mathbf{n})$ and directly available from geological maps, geological understanding, local outcrops, and nearby boreholes. The second type of information is indirect and relates observations, for example geophysical data such as EM measurements, to the model parameters through a *likelihood*.

The posterior probability distribution $\sigma(\mathbf{m}, \mathbf{n})$ can be calculated through conjunction of information as (Tarantola and Valette, 1982a; Sivia and Skilling, 2006; Mosegaard and Tarantola, 2002; Hansen et al., 2016)

$$\sigma(\mathbf{m}, \mathbf{n}|H) = \frac{\rho(\mathbf{m}, \mathbf{n}|H)\, L(\mathbf{m}, \mathbf{n}|H)}{E(H)}. \tag{1}$$

$E(H)$ is the evidence, also known as the *marginal likelihood* (MacKay, 1992), representing the normalization constant ensuring that the posterior probability distribution is properly normalized and is given by

$$E(H) = \iint L(\mathbf{m}, \mathbf{n}|H) \cdot \rho(\mathbf{m}, \mathbf{n}|H)\, d\mathbf{m}\, d\mathbf{n}. \tag{2}$$

$E(H)$ quantifies how well hypothesis H explains the observed data. In most practical applications of posterior sampling methods, such as MCMC, the evidence need not be computed explicitly because the sampling is performed on the unnormalized posterior (Metropolis et al., 1953; Mosegaard and Tarantola, 1995). However, the evidence becomes essential when performing hypothesis testing or model comparison, where the relative probabilities of competing models are evaluated via Bayes factors (Sambridge et al., 2006). In `INTEGRATE`, the evidence is estimated efficiently as a by-product of the sampling procedure and used to quantify the relative support for different geological hypotheses.

The formulation in Equation 1 generalizes the approach used by Tarantola and Valette (1982a) by explicitly conditioning all probabilities on the hypothesis H, which refers to a specific framework that defines the complete context for an inversion. This includes a particular choice of model parameterization, a specific prior probability distribution $\rho(\mathbf{m}, \mathbf{n}|H)$, and a specific likelihood function $L(\mathbf{m}, \mathbf{n}|H)$. This conditioning acknowledges that all information exists within some context or framework, and as Sivia and Skilling (2006) argues, every piece of information, whether prior knowledge or data-derived likelihood, is inherently dependent on underlying assumptions and context. In the following, conditioning on H will be implicit, so we write $\rho(\mathbf{m}, \mathbf{n} \mid H)$ simply as $\rho(\mathbf{m}, \mathbf{n})$. Since $\mathbf{k} = [\mathbf{m}, \mathbf{n}]$, we further abbreviate this as $\rho(\mathbf{k})$. The same implicit conditioning applies to the likelihood and posterior, so $L(\mathbf{m}, \mathbf{n} \mid H)$ and $\sigma(\mathbf{m}, \mathbf{n} \mid H)$ will be written simply as $L(\mathbf{k})$ and $\sigma(\mathbf{k})$.

2.2. Methodology

In order to sample from the posterior probability distribution $\sigma(\mathbf{k})$ as defined in Eq. 1, a variation of the extended rejection sampler with lookup tables, as presented by Hansen (2021), is used, as it has been demonstrated to be numerically efficient, can handle arbitrarily complex prior information, and, as will be demonstrated, can be used for hypothesis testing.

2.2.1. The extended rejection sampler

One of the simplest sampling algorithms for sampling a probability distribution, such as $\sigma(\mathbf{k})$, is the rejection sampler. It only requires that one can (a) generate a sample from a proposal distribution $h(\mathbf{k})$ (often chosen as the uniform distribution) and (b) accept that model as a realization of $\sigma(\mathbf{k})$

with a probability $P_{acc} = c_P \frac{\sigma(\mathbf{k})}{h(\mathbf{k})}$, where c_P is a normalization constant ensuring P_{acc} is never larger than 1. Hansen (2021) describes a variation of the rejection sampler, the extended rejection sampler, designed to sample from a probability distribution proportional to the product of two probability distributions, such as in Eq. 1, when one can sample from one probability distribution, e.g. $\rho(\mathbf{k})$, and evaluate the other, e.g. $L(\mathbf{k})$.

We expect observed data $\mathbf{d}_{obs}$ can be represented as the outcome of a forward model

$$\mathbf{d} = g(\mathbf{k}), \tag{3}$$

and a noise term $n(\mathbf{k})$, such that

$$\mathbf{d}_{obs} = g(\mathbf{k}) + n(\mathbf{k}). \tag{4}$$

Following Tarantola (2005), the likelihood $L(\mathbf{k})$ is defined by the probability density of the data, ρ_D, evaluated at the modeled data $g(\mathbf{k})$. Assuming additive noise described by the distribution f_{noise}, this corresponds to evaluating the noise distribution at the residual:

$$L(\mathbf{k}) = f_{noise}(g(\mathbf{k}), \mathbf{d}_{obs}) \tag{5}$$

This formulation explicitly allows for general noise models f_{noise} that are not necessarily centered at zero (e.g., in the presence of systematic bias).

The specific distribution of f_{noise} depends on the type of noise in the data. For example, if the data are continuous and the noise is Gaussian, f_{noise} is the multivariate Gaussian distribution, and if the data are discrete/categorical, f_{noise} can be the multinomial distribution. Thus, in order to evaluate $L(\mathbf{k})$ for a specific set of model parameters $\mathbf{k}^*$, one needs to (a) compute the forward response, Eq. 3, and (b) evaluate the noise model.

2.2.2. Implementing the extended rejection sampler

The extended rejection sampler can be implemented by running the following steps:

1. **Propose** a model $\mathbf{k}^*_{pro}$, as a realization of $\rho(\mathbf{k})$.
2. **Compute the forward** response, $\mathbf{d}^*_{pro}$ using Eq. 3.
3. **Compute** the likelihood L_{pro} using Eq. 5.
4. **Accept** $\mathbf{k}^*_{pro}$ as a realization of $\sigma(\mathbf{k})$ with probability P_{acc} (proportional to $L(\mathbf{k}^*_{pro})$)

$$P_{acc} = \left(\frac{L(\mathbf{k}^*_{pro})}{c} \right)^{1/T}, \tag{6}$$

where c is a normalization constant satisfying $c \geq \max(L(\mathbf{k}^i))$ for $i = 1, \ldots, N$. i.e. c must be equal to or larger than the maximum of all computed values of $L(\mathbf{k}^i)$. As a generalization of Hansen (2021), the parameter T, referred to as the annealing temperature, is introduced that can be used to control the weight of the data. Repeating steps 1–4 will lead to a sequence of accepted models that represent realizations of the posterior distribution.

Note that using the extended rejection sampler requires only that one can generate realizations from the prior distribution $\rho(\mathbf{k})$ and and evaluate the likelihood $L(\mathbf{k})$. It is not required to be able to evaluate neither the prior probability distribution $\rho(\mathbf{k})$ nor the posterior probability distribution $\sigma(\mathbf{k})$. It is enough that an algorithm exists that can generate realizations from $\rho(\mathbf{k})$. This is particularly useful when using complex prior models, such as multiple-point statistics (Hansen et al., 2008) or object-based models (Linde et al., 2015), where it may not be possible to evaluate $\rho(\mathbf{k})$ directly, but where one can generate realizations of $\rho(\mathbf{k})$ using for example a training image or an object-based algorithm.

Lookup tables The extended rejection sampler can be implemented efficiently using pre-computed lookup tables containing realizations of prior models and their corresponding forward responses. This approach offers significant computational advantages over traditional sampling methods, particularly for localized inverse problems, and can be implemented in three main steps:

1 **Create a lookup table** by generating N realizations from the prior distribution $\rho(\mathbf{m}, \mathbf{n})$, stored as $[\mathbf{M}^*, \mathbf{N}^*]$, and computing their corresponding data responses $\mathbf{D}^*_i = g(\mathbf{m}_i, \mathbf{n}_i)$ for $i \in \{1, \ldots, N\}$. The resulting collection of responses is denoted $\mathbf{D}^* = \mathbf{D}^*_1, \ldots, \mathbf{D}^*_N$.* Finally, the model-data pairs $[\mathbf{M}^*, \mathbf{N}^*, \mathbf{D}^*]$ are stored (in memory or on disk).

2 **Compute the likelihood** $\mathbf{L}^* = [L(\mathbf{m}_i, \mathbf{n}_i), \ldots, L(\mathbf{m}_N, \mathbf{n}_N)]$ for all N stored model-data pairs using the observed data $\mathbf{d}_{obs}$. The maximum likelihood value is used to determine the normalization constant c.

2a Optionally compute or select a specific annealing temperature T.

3 **Sample the posterior** by randomly selecting models from the lookup table with probability proportional to their acceptance probability P_{acc} (Eq. 6).

For localized inverse problems, such as 1D electromagnetic soundings where thousands of independent inversions are required, the same lookup table can be reused across different locations, such that only steps 2–3 need to be repeated for each dataset.

2.2.3. Evidence calculation using lookup tables

As the likelihood is computed for all models in the lookup table, an estimate of the evidence (Eq. 2) can be obtained at negligible extra computational cost, as the mean likelihood of a (large) sample of N realizations of the prior:

$$E(H) \approx \frac{1}{N} \sum_{i=1}^{N} L(\mathbf{m}^*_i, \mathbf{n}^*_i). \tag{7}$$

The larger the sample size N, the more accurate the approximation.

2.2.4. *Annealing temperatures*

In some cases one will only accept a few different models from the posterior using the extended rejection sampler, and in extreme cases only one model. This happens when the acceptance probability, Eq. 6, is much higher for one model than for all others. This can be due to the data being very informative, or when the amplitude of the assumed noise is lower than the real noise, and the likelihood function is spiky. In order to avoid generating too few realizations from the posterior to obtain meaningful posterior statistics, an annealing temperature T can be introduced in Eq. 6, and can be used if needed.

The annealing temperature T can be used to control the weight of the data in the inversion process. Figure 1 illustrates the effect of the annealing temperature on the probability distribution being sampled, given a simple 1D prior and likelihood as an example.

When $T = 1$, the algorithm will sample from the true posterior $\sigma(\mathbf{k})$ (if N is high enough) (solid black line in Figure 1). When $T \to 0$, the algorithm will tend to sample a delta distribution at the maximum of $L(\mathbf{m})$. Using $T < 1$ will lead to overfitting the data, which is not advised (and therefore not shown in Figure 1). When $T > 1$, the algorithm will sample an approximation to the posterior distribution. As T increases, the acceptance probability will increase, and the influence of the likelihood decreases, leading to an effective posterior distribution that lies between the true posterior and the prior. In the extreme case when $T \to \infty$, $P_{acc} = 1$, and the algorithm will sample directly from the prior distribution $\rho(\mathbf{k})$ (dashed line in Figure 1). The thin black lines in Figure 1 illustrate intermediate distributions at different T values.

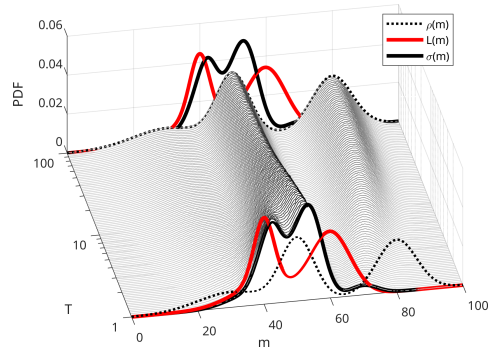

Figure 1: Effect of annealing temperature on the posterior probability distribution $\sigma(\mathbf{m})$ being sampled, given a simple 1D prior $\rho(\mathbf{m})$ and likelihood $L(\mathbf{m})$ as an example.

Automatic tuning of the annealing temperature One can choose to automatically select the annealing temperature, T_{auto}, to ensure, for example, a minimum number of models, $N_{T_{\min}}$, having an acceptance probability above some minimum threshold, $P_{acc_{lev}}$. This can be obtained using the acceptance probability derived from the likelihood values in the lookup table.

Given the log-likelihood values $\mathbf{logL} = [\log(L_1), \log(L_2), \ldots, \log(L_N)]$ the automatic temperature can be computed as follows. First, normalize the log-likelihood values by subtracting the maximum:

$$\log(L_i^{norm}) = \log(L_i) - \max(\mathbf{logL}) \tag{8}$$

Next, sort the normalized log-likelihood values in ascending order to obtain the sorted array $\mathbf{logL}^{sorted}$. From this sorted list, select the $(N_{T_{\min}}+1)$-th element from the end (i.e., the $(N_{T_{\min}}+1)$-th largest value), denoted as $\log L_{lev}^{norm}$. The automatic temperature is then computed as:

$$T_{auto} = \max\left(1, \frac{\log L_{lev}^{norm}}{\log(P_{acc_{lev}})}\right), . \tag{9}$$

where $P_{acc_{lev}}$ is the desired acceptance probability threshold (e.g., 0.2), and $N_{T_{\min}}$ is the number of models that should have acceptance probabilities above this threshold (e.g., 10). The temperature is constrained to be at least 1 to avoid overfitting the data.

3. Implementation

The INTEGRATE framework is implemented in Python but is not tied to any specific programming language. All data exchange between its components is handled through HDF5 files, which serve as a common interface between independent processing modules. This design allows each algorithmic component, including prior generation, forward modeling, posterior sampling, and computation of summary statistics, to operate independently and to be replaced by alternative implementations without requiring changes to the rest of the system, as long as the same HDF5 structure is respected. As a result, any external software that can read and write HDF5 files can interact seamlessly with INTEGRATE.

The package implements the localized extended rejection sampler described in Section 2.2.1 and is designed to be efficient, modular, and transparent. A typical workflow involves four main steps:

1. Preparation of the observed data.
2. Construction of a lookup table containing realizations of the prior $\rho(\mathbf{k})$ and corresponding forward responses $g(\mathbf{k})$.
3. Evaluation of the likelihood and subsequent sampling of the posterior distribution.
4. Computation of posterior statistics (mean, mode, entropy) and Bayesian evidence.

All information is stored in three HDF5 files:

- **DATA.h5** Contains the observed data, associated metadata, and noise model information. Each dataset (e.g., an EM sounding or well log) is stored in a dedicated group with attributes specifying the noise model (Gaussian or multinomial) and optional geometry (e.g., coordinates and elevation).
- **PRIOR.h5** Holds realizations of the prior model parameters $\rho(\mathbf{m})$ and their corresponding forward responses

$g(\mathbf{m})$. These form the lookup table used during posterior sampling. Model parameters may be continuous or discrete, enabling flexible representation of geological prior information.

- **POST.h5** Contains the results of the inversion, including indices of accepted prior realizations, annealing temperature, estimated evidence, and posterior summary statistics for all model parameters. From these, pointwise means, modes, and entropies are computed automatically.

Parallelization is implemented through shared-memory multiprocessing, allowing each independent inversion task (e.g., one sounding) to be processed concurrently. The `HDF5`-based design ensures efficient scaling and minimal communication overhead, making it suitable for large-scale applications.

Further details, including the file structure and usage examples, are provided in the online documentation at `https://cultpenguin.github.io/integrate_module/` and in the source code repository at `https://github.com/cultpenguin/integrate_module`.

4. Results

The INTEGRATE package has been developed as part of the INTEGRATE research project[1], which focuses on integrating geophysical electromagnetic data, well log data, and structural prior information, to assists decision makers locating raw materials (Hansen and Gulbrandsen, 2024).

The INTEGRATE package allows seamless access to a number of reference data sets, and the documentation contains many examples of different cases illustrating the different capabilities of the package, such as joint inversion of multiple datasets, different noise models, different data types (continuous and discrete), different prior models, and so on. The documentation is available at `https://cultpenguin.github.io/integrate_module/`. Here we choose to exemplify the package using tTEM data from Daugaard, Denmark.

4.1. Case study - tTEM data from Daugaard, Denmark, with two hypotheses

All data were collected on a single day with the same tTEM system (Auken et al., 2019), using a single system calibration. After processing in AGS Workbench[2] (Auken et al., 2009) 11693 dual-moment soundings are available, each representing up to 40 dB/dT measurements from both a low (14 gates) and high moment (26 gates).

The 11693 observed data, as well the associated uncorrelated Gaussian uncertainties, represented by a standard deviation that is the sum of 3% relative error and an absolute base error level, are stored in the `HDF5` file `DATA_Daugaard.h5`. Figure 2 shows the locations of the 11693 soundings, and the total number of non-NaN data available at each location, covering an area of approximately 25 km^2. Some gates are removed as part of processing and therefore the number of data per sounding varies between 10 and 25.

As the noise is assumed to be Gaussian, we use the reduced chi-squared statistic to quantify the data fit:

$$\chi^2_v = \frac{1}{N_d}(\mathbf{d} - \mathbf{d}_{obs})^T \mathbf{C}_D^{-1}(\mathbf{d} - \mathbf{d}_{obs}). \quad (10)$$

In the present case $\mathbf{C}_D$ is a diagonal matrix with measurement variance in the diagonal. $\chi^2_v < 1$ implies that the data are fit better than the noise levels suggest (i.e., overfitting), while $\chi^2_v > 1$ implies an underfit. A value of $\chi^2_v \approx 1$ indicates that the data residuals of the accepted models are distributed according to the specified Gaussian noise model.

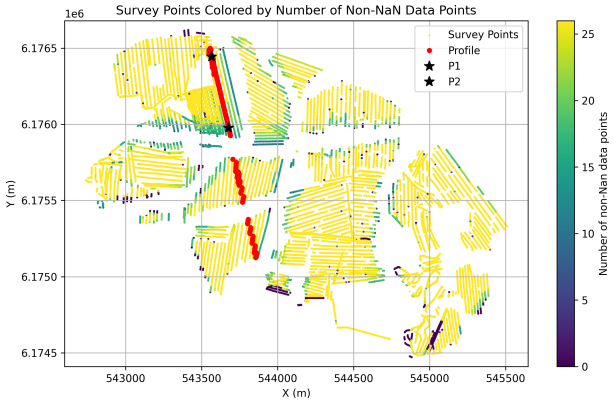

Figure 2: Daugaard survey area. Black stars indicate single locations analyzed below. Red dots indicate the location of the cross sections shown below. Colors indicate the number of non-NaN data per sounding.

4.2. The prior models

The survey area at Daugaard is located in a region of Denmark that is strongly influenced by past glacial activity. A characterizing feature of the regional glacial setting are paleo valleys filled in with younger sediments, also known as buried valleys. These valleys are often infilled with coarse materials such as sand or gravel, which makes them great bodies for groundwater reservoirs or aquifers, and a potential source for construction aggregates. Large parts of the near-surface of Denmark contain networks of these buried valleys that are well documented and studied (Jørgensen et al., 2010). In addition, the existence of resistivity-lithology studies (e.g. Barfod et al. (2016)) allows setting up probabilistic models that describe the expected relation between lithology and resistivity, and the subsurface architecture, within and outside buried valleys.

We have used this information to set up two prior models: one for the case of a buried valley sequence, $\rho_{\text{inside}}(\mathbf{m}, \mathbf{n})$, and one for the case of an outside of valley sequence, $\rho_{\text{outside}}(\mathbf{m}, \mathbf{n})$. The `GeoPrior1D` code (Nørgaard et al., 2026) was used to construct the two prior models, following the approach described in Madsen et al. (2023). The process begins by defining a layered 1D model representing variations in lithology, $\rho(\mathbf{n})$. Realizations of this lithology are generated in a 90-

[1] https://integrate.nu/
[2] https://www.seequent.com/products-solutions/ags-workbench/

layer model with layers of 1 m thickness. Subsequently, realizations of the corresponding resistivity are sampled from a chosen relationship between lithology and resistivity, i.e., from $\rho(\mathbf{m}|\mathbf{n})$. Details in the use of the `GeoPrior1D`, with an example from Daugaard, code can be found in Nørgaard et al. (2026).

Initially we consider a simple mixture of the two prior models, with equal weight, i.e.,

$$\rho(\mathbf{k}) = 0.5\rho_{inside}(\mathbf{k}) + 0.5\rho_{outside}(\mathbf{k}) \tag{11}$$

We consider 1.000.000 realizations of each prior model, leading to a total of 2.000.000 realizations when combining the two prior models. In Appendix A, Figures A01, A02, and A03 show summary statistics and 100 realizations of $\rho_{\text{inside}}(\mathbf{k})$, $\rho_{\text{outside}}(\mathbf{k})$, and $\rho(\mathbf{k})$ respectively. We use GA-AEM (Brodie, 2020) to compute the forward response of all prior models, as it provides accurate 1D TEM forward simulations, is computationally efficient, runs on multiple platforms, and is available under an open-source license (Falk et al., 2025b).

4.3. Rejection sampling of the posterior distribution

Below, we illustrate several examples of using the extended rejection sampler to sample from the posterior distribution based on the mixed prior model and the observed data from Daugaard, Denmark.

4.3.1. Automatic annealing

Initially, the extended rejection sampler is executed using automatic estimation of the annealing temperature, as described in Eq. 9, with $P_{\text{acc,lev}} = 0.1$ and $N_{T_{\text{min}}} = 30$. Thus, the annealing temperature is automatically selected to ensure that at least 30 models have an acceptance probability above 0.1. It is then used to sample the posterior distribution based on the mixed prior model and the observed data, as described above. Once the posterior distribution has been sampled, joint realizations of $\sigma(\mathbf{m}, \mathbf{n})$ are readily available.

Figure 3 compares the observed data with the forward responses of 200 realizations of the prior (prior data) and posterior (posterior data) for locations P1 and P2 shown in Figure 2.

Comparison of observed and prior data reveals good consistency for location P1, as there is overlap between prior and observed data. For location P2, the overlap is smaller, suggesting potential inconsistency and indicating that the data at P2 are more difficult to fit. In addition, 16 data are available at P1, while 26 data are available at P2, making the data at P2 more informative.

This is reflected in the estimated annealing temperatures of $T = 1.7$ for P1 and $T = 3.9$ for P2, indicating that fewer models have significant acceptance probabilities for P2 than for P1. At the same time, the reduced chi-squared statistic, Eqn 10, of the accepted posterior models is 1.5 for P1 and 1.1 for P2, suggesting a data fit consistent with the noise model, with a slight tendency of underfitting.

Figures 4 and 5 show posterior marginal statistics such as the median and standard deviation from $\sigma(\mathbf{m})$, and the mode and entropy from $\sigma(\mathbf{n})$, i.e., from $\sigma(\mathbf{m})$ and $\sigma(\mathbf{n})$, respectively, along the cross-section shown in Figure 2. Entropy is computed with a logarithmic base of N_{classes}, such that a value of 1 represents a uniform (non-informative) posterior marginal distribution, and a value of 0 represents a fully informative posterior marginal distribution (i.e., the posterior probability of one class is 1, and all others are 0). Other statistics, such as mean, percentiles, and class probabilities, are also available in the `POST.h5` file but are not shown here.

N	T (P1)	T (P2)	χ^2_ν (P1)	χ^2_ν (P2)
10^3	16.7	219	4.6	26.4
10^4	8.5	44.0	3.0	7.7
10^5	2.0	17.7	1.7	3.1
2×10^6	3.8	3.9	1.5	1.1

Table 1
Automatic annealing temperature, T, and reduced chi-squared statistic χ^2_ν, for different sizes of the prior sample, N, for locations P1 and P2 in Figure 2.

4.3.2. Automatic annealing and the size of the prior sample

The automatic annealing temperature ensures that a minimum number of models are accepted to represent the posterior, thereby allowing meaningful posterior statistics to be computed. It depends on the size of the prior sample, as a larger sample will contain more models with high likelihood values and, consequently, more models with high acceptance probabilities.

Figure 6 shows the data fit for location P2 using different sizes of the prior sample, $N = [10^3, 10^4, 10^5]$. The annealing temperature is automatically selected in each case, and the corresponding values are listed in Table 1 (together with those for location P1) along with the reduced chi-squared statistic (χ^2_ν). As expected, the annealing temperature decreases with increasing prior sample size. For data locations where the data are more difficult to fit within their assumed uncertainty (as for location P2; see discussion above), the estimated annealing temperature is higher. At the same time, the χ^2_ν decreases with increasing prior sample size, as a better data fit can be achieved, on average, when the sample size is larger.

Figure 7 shows the median resistivity at a depth of $z = 45$ m for different prior sample sizes, $N = [10^3, 10^4, 10^5, 2\times 10^6]$. Figure 8 shows the corresponding mode of the lithology at the same depth. These statistics are remarkably stable with respect to the size of the prior sample, suggesting that even a prior sample with $N = 10^4 \rightarrow 10^5$ realizations may be sufficient to robustly estimate key statistics of the posterior distribution.

4.3.3. Fixed temperature

The main motivation for introducing the automatic annealing temperature is to ensure that a minimum number of models are accepted from the posterior, thereby allowing meaningful posterior statistics to be computed. Alternatively, one can choose to use a fixed annealing temperature,

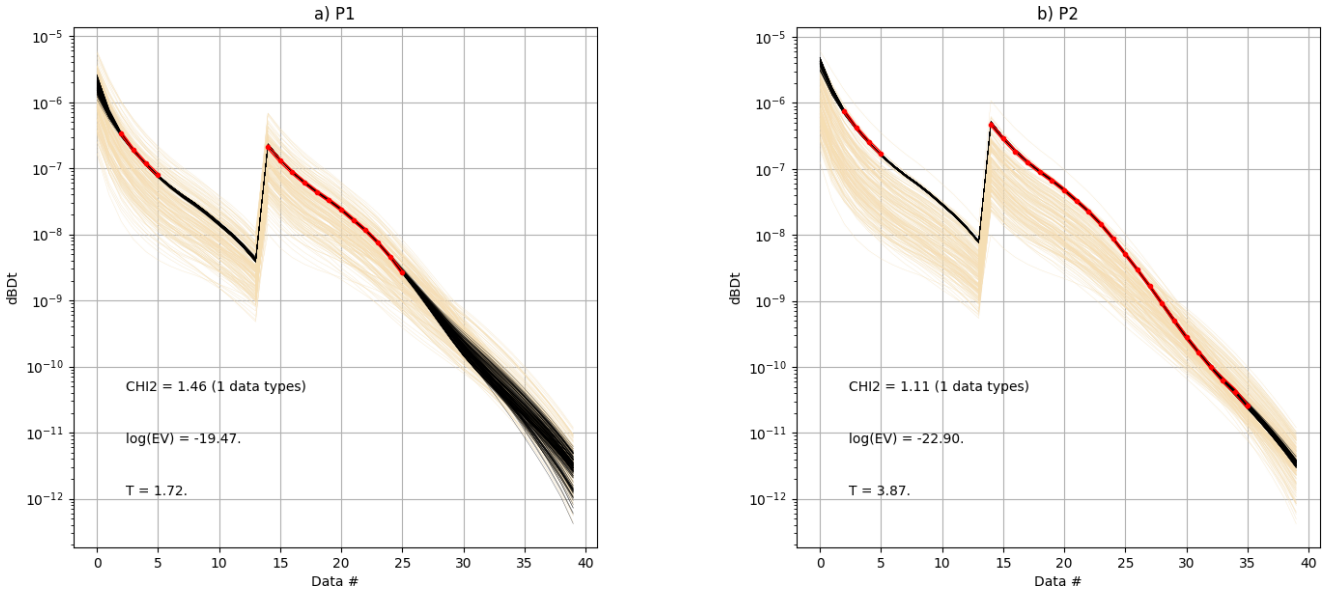

Figure 3: Prior (brown), posterior (black), and observed data (red dots), data uncertainty (red lines), for locations left (P1) and right (P2) in Figure 2, using the mixed prior model and automatic annealing temperature.

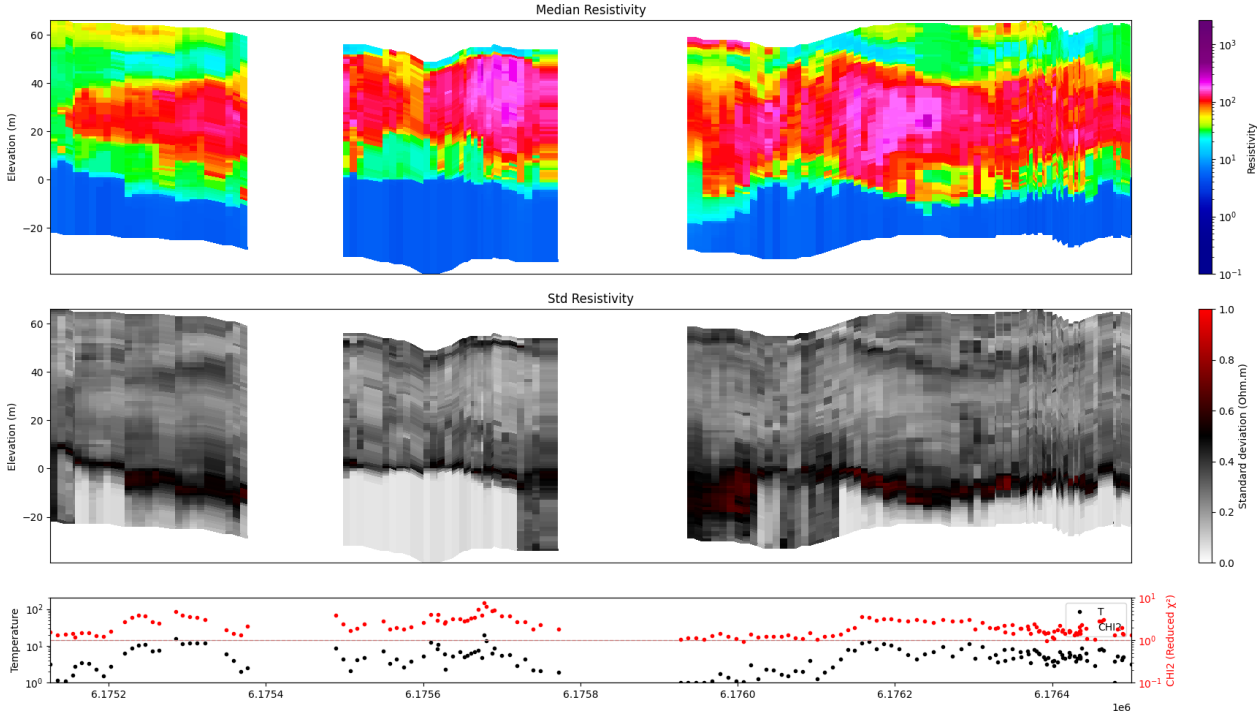

Figure 4: Cross section of the mean (top) and standard deviation (middle) of the posterior resistivity, $\sigma(\mathbf{m})$, using the mixed prior model and automatic annealing temperature. The bottom plot shows the used annealing temperature T as well as the chi-squared statistic (χ^2_v). The location of the cross section is shown in Figure 2.

T, for all data sets, which may be useful in certain cases.

Figure 9 shows the posterior median resistivity and mode of lithology at a depth of $z = 45$ (as in Figures 7- 8, which varies the size of the prior sample) using different fixed annealing temperatures, $T = [1, 10, 100]$, with a lookup-table of size $N = 2 \times 10^6$. As seen, when $T = 1$, the posterior statistics may exhibit artifacts due to the limited number of accepted models used for statistical estimation. Increasing the annealing temperature (analogous to increasing the assumed noise level) leads to more models with relatively high acceptance probabilities, and therefore to a larger number of accepted models and more robust posterior statistics.

We recommend using the automatic annealing temperature as the default, as it adapts naturally to the local uncertainty and increases the temperature only where needed.

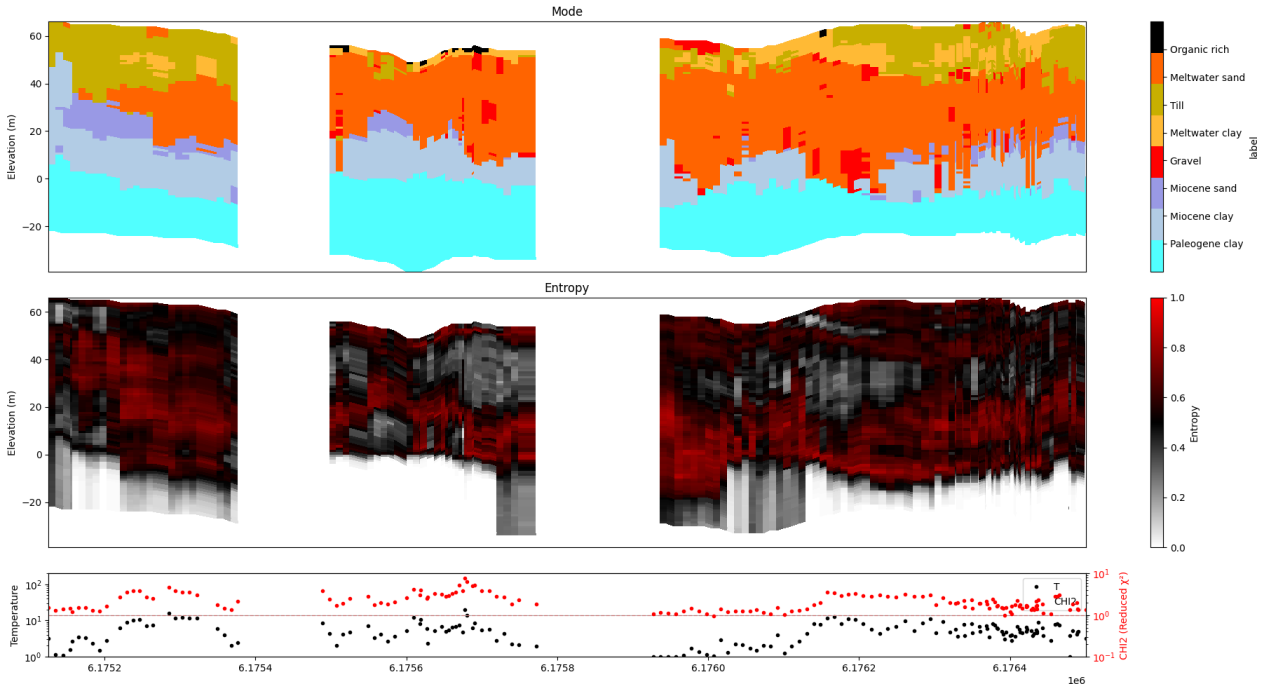

Figure 5: Cross section of the mode (top) and entropy (middle) of the posterior lithology, $\sigma(\mathbf{n})$, using the mixed prior model and automatic annealing temperature. The bottom plot shows the used annealing temperature T as well as the chi-squared statistic (χ^2_v). The location of the cross section is shown in Figure 2.

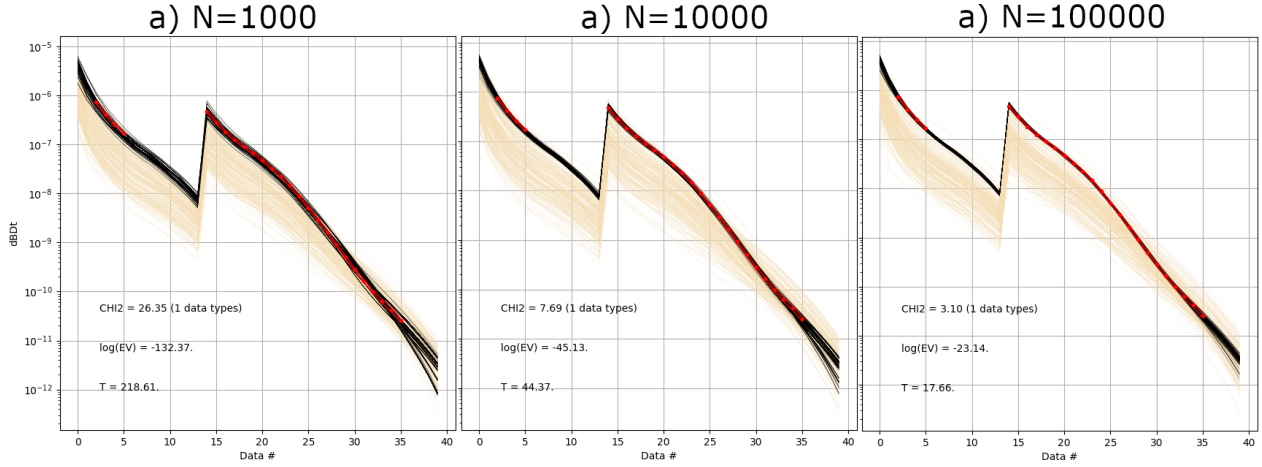

Figure 6: Observed data (red) with 200 realizations of prior and posterior data (brown and black, respectively) for location P2 in Figure 2, using a) $N = 10^3$, b) $N = 10^4$, and c) $N = 10^5$ prior realizations. See also Figure 3 for $N = 2 \times 10^6$.

4.3.4. Hypothesis testing

There are two main ways to apply hypothesis testing within the INTEGRATE framework. The first approach is to use the obtained posterior samples from the mixture prior $\rho(\mathbf{k})$ (Eq. 11) and count the frequency of accepted models originating from each hypothesis (as defined by the corresponding prior model type). For example, if 100 realizations are accepted and 30 correspond to hypothesis H_{inside}, the posterior probability of H_{inside} is simply $\sigma_{\text{mixture}}(H_{\text{inside}}) = 30/100 = 0.3$. The posterior probability of H_{inside} obtained in this way by directly from sampling the mixture posterior is shown in Fig. 10 for two cases: using the original noise level and using a noise level inflated by a factor of four.

The second approach is to treat each hypothesis separately amd explicitly use the estimate of the evidence. For multiple hypotheses H_i ($i = 1, \ldots, N_h$) with prior probabilities $\rho(H_i)$ satisfying $\sum_{i=1}^{N_h} \rho(H_i) = 1$, the posterior probability of each hypothesis is given by

$$\sigma(H_i) = \frac{E(H_i)\,\rho(H_i)}{\sum_{j=1}^{N_h} E(H_j)\,\rho(H_j)}. \tag{12}$$

In practice, one can run the extended rejection sampler separately for each hypothesis, i.e., sample $\sigma_{\text{inside}}(\mathbf{k})$ and $\sigma_{\text{outside}}(\mathbf{k})$

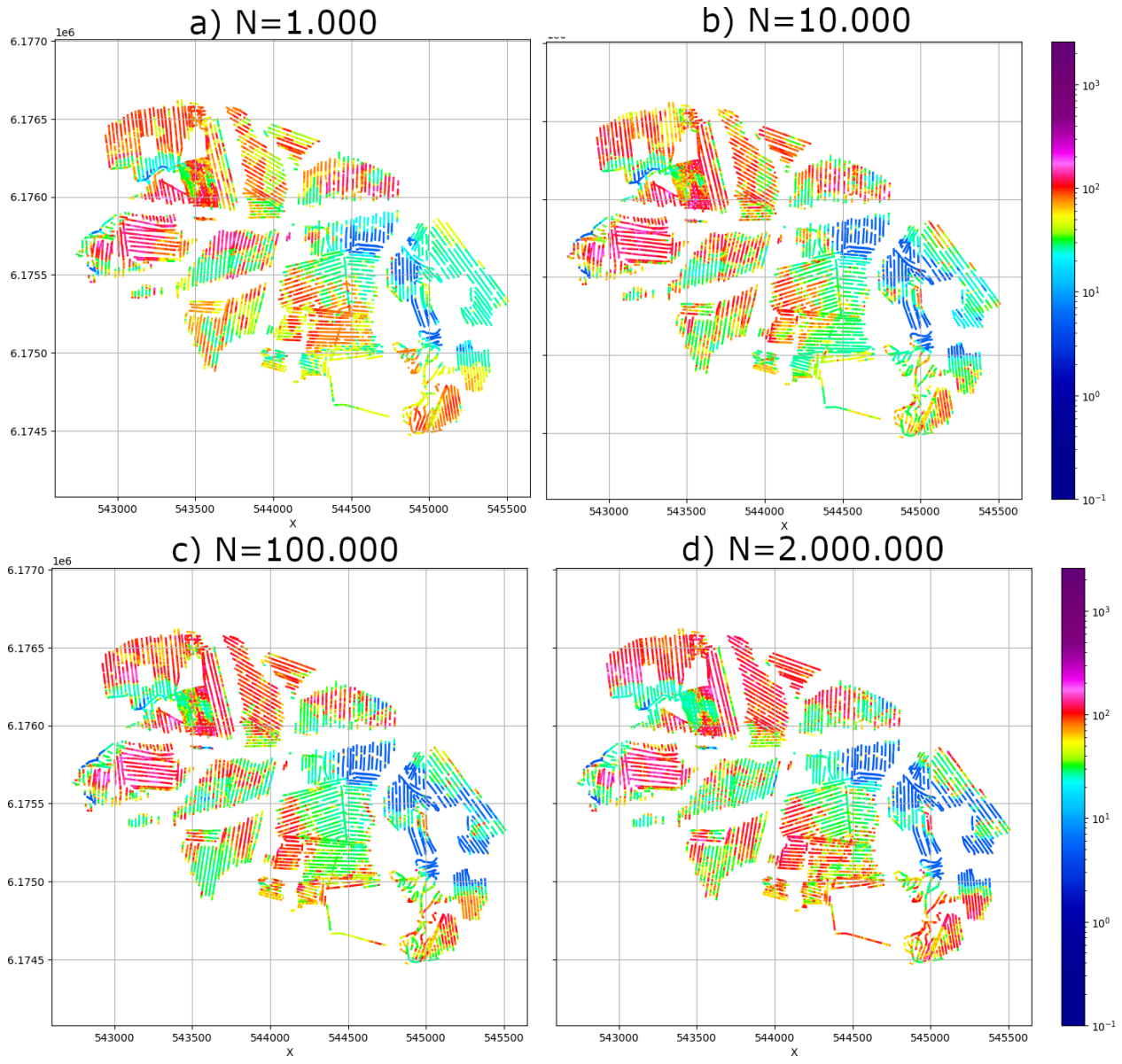

Figure 7: Posterior median of resistivity $\sigma(\mathbf{m})$ at a depth of $z = 45$ m, using different sample sizes a) $N = 10^3$, b) $N = 10^4$, c) $N = 10^5$, and d) $N = 2 \times 10^6$prior realizations.

independently, compute the evidence for each, and then use Eq. 12 to determine the posterior probability of each hypothesis. The posterior probability of H_{inside} obtained using Eq. 12 from the samples $\rho_{\text{inside}}(\mathbf{k})$ and $\rho_{\text{outside}}(\mathbf{k})$ is shown in Fig. 11 for two cases: using the original noise level and using a noise level inflated by a factor of four.

For all results shown in Figs. 10 and 11, similar areas of relatively high probability for H_{inside} can be identified. However, considerably more noise is observed in the results obtained using explicit evidence computation (Fig. 11a) than in those obtained directly from the mixture prior (Fig. 10a) when using the original (low) noise level.

In principle, using the same noise level and annealing temperature should yield equivalent results (Sambridge et al., 2006). However, evidence computation is independent of the annealing temperature, whereas the acceptance ratio is strongly affected by it. By inflating the noise level by a factor of four, both methods produce very similar results, as expected, since the effective annealing temperature will be close to 1 everywhere (see Figs. 10b and 11b) and quite similar to those obtained from the mixture prior using the original noise level (Fig. 10a).

The dashed lines in Figures 10- 11 indicates the location of the boundaries of a buried valley interpreted from a combination of inverted TEM data (using AGS Workbench[3]) and borehole data. The existence of the buried valley was established before and independently of the presented inversion results. The evidence-based results show good correspondence with the interpreted boundaries, demonstrating the ability of both approaches to discriminate effectively be-

[3] https://www.seequent.com/products-solutions/ags-workbench/

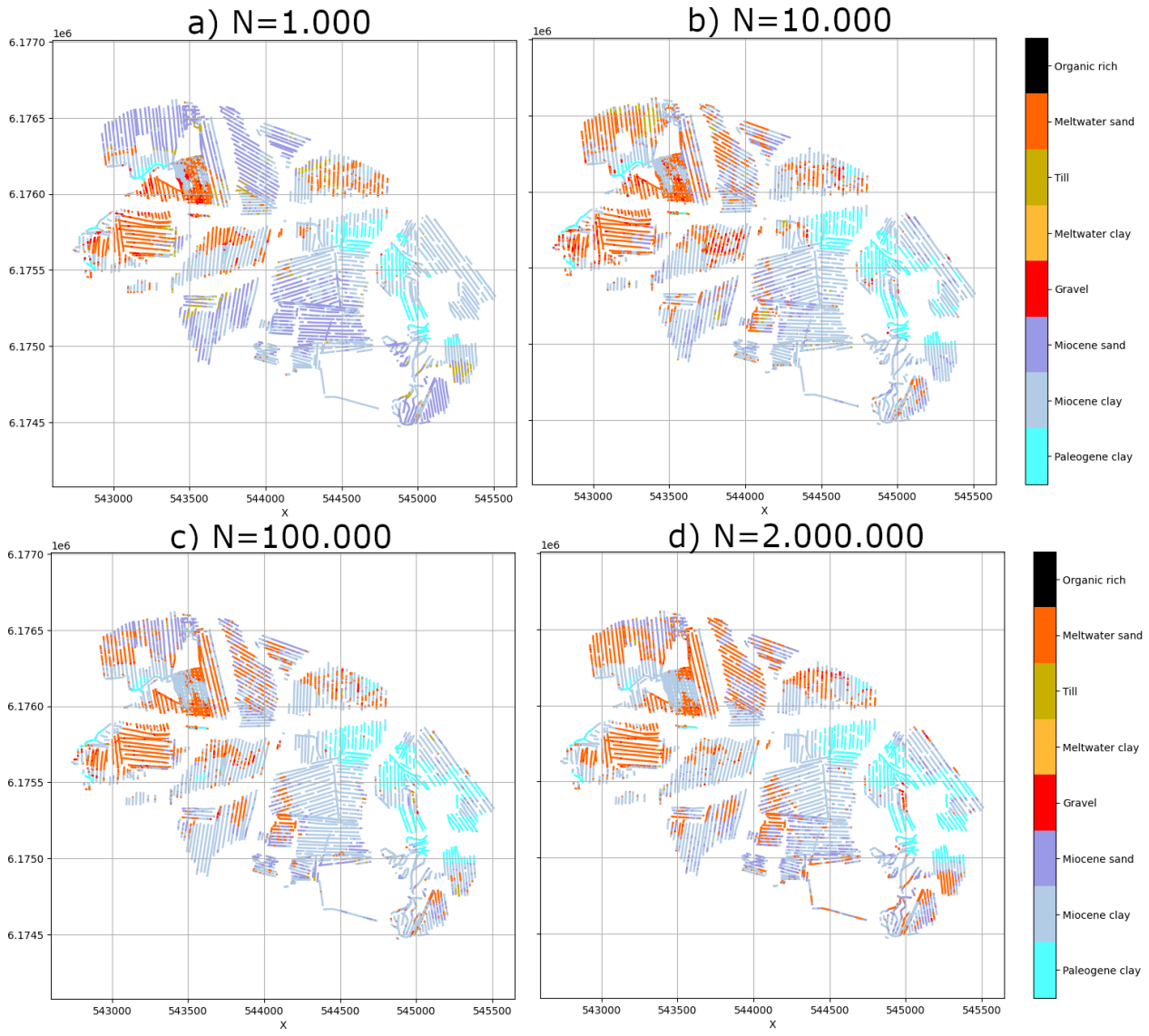

Figure 8: Posterior mode of lithology $\sigma(\mathbf{n})$ at a depth of $z = 45$ m, using different sample sizes a) $N = 10^3$, b) $N = 10^4$, c) $N = 10^5$, and d) $N = 2 \times 10^6$prior realizations.

tween the two hypotheses.

5. Discussion

The INTEGRATE package provides a flexible and efficient framework for localized probabilistic inversion using an extended rejection sampler that allows handling arbitrarily complex prior and likelihood information, as demonstrated above using tTEM data from the Daugaard test site in Denmark.

5.1. Advantages of the extended rejection sampler with complex priors

A key feature of INTEGRATE is its ability to incorporate arbitrarily complex prior information without requiring random-walk sampling of the prior space. Most existing methods, both deterministic and probabilistic, rely on simple, fixed prior models (Auken et al., 2005; Minsley, 2011; Foks and Minsley, 2020). In contrast, the extended Metropolis algorithm (Hansen et al., 2013; Hansen and Minsley, 2019) can accommodate more flexible priors, but still requires computationally expensive sampling through a random walk in model space. The extended rejection sampler implemented in INTEGRATE avoids this limitation by requiring only that independent realizations of the prior can be generated, as provided by geostatistical simulation methods (Deutsch and Journel, 1992; Goovaerts, 1997; Strebelle, 2002; Mariethoz and Caers, 2014) and sequential Gibbs sampling (Hansen et al., 2012).

This approach offers two key advantages related to independence. First, generating independent prior realizations is typically much easier than designing an efficient random walk through complex, multimodal model spaces, making it more practical to incorporate sophisticated prior information. Second, rejection sampling produces independent pos-

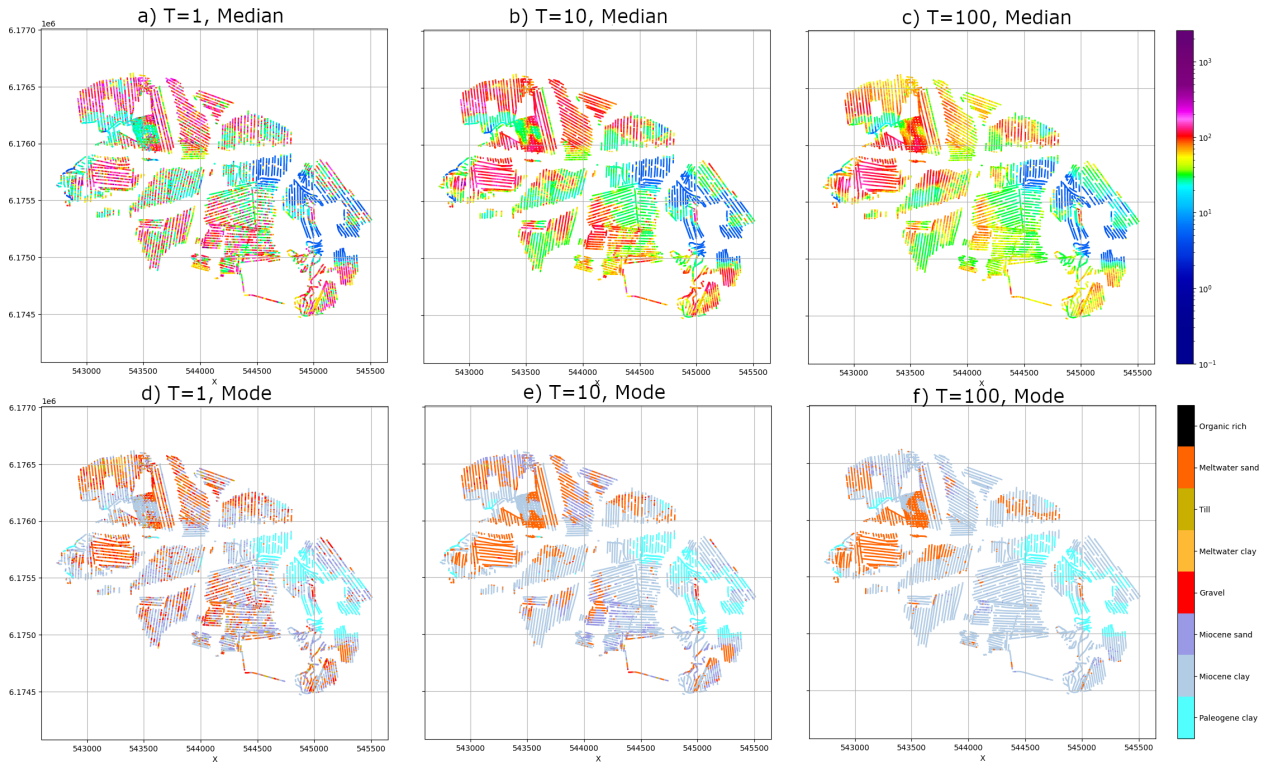

Figure 9: Posterior median of resistivity $\sigma(\mathbf{m})$) (a,b,c) and posterior mode of lithology $\sigma(\mathbf{n})$ (d,e,f) at a depth of $z = 45$ m, using fixed annealing temperatures a,d) $T = 1$, b,e) $T = 10$, and c,f) $T = 100$.

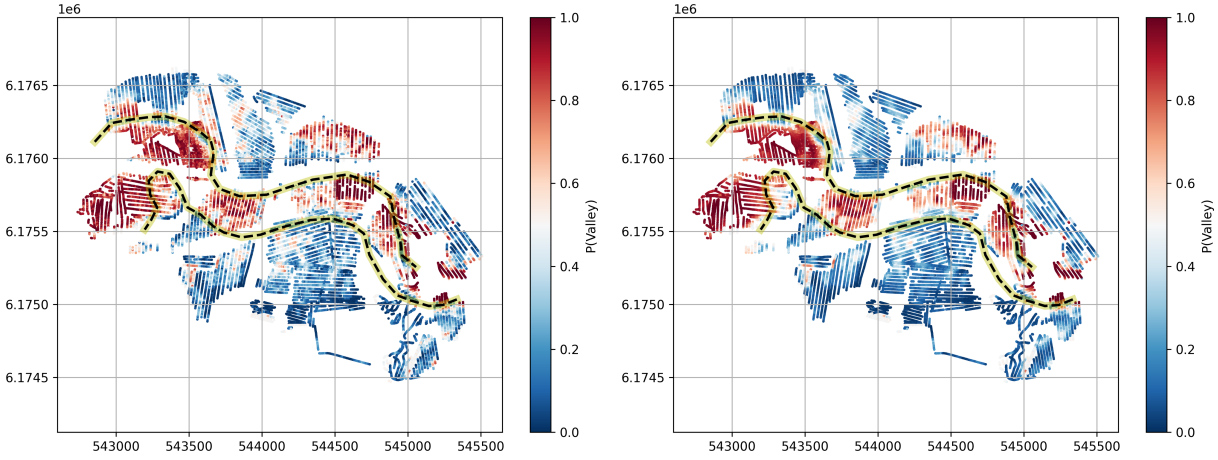

(a) $\sigma(H_{inside})$ using N=2×10^6.

(b) $\sigma(H_{inside})$ using N=2×10^6, and noise inflated by a factor of 4.

Figure 10: Comparison of $\sigma_{mixture}(H_{inside})$ using different noise levels, obtained directly from posterior hypothesis type from the mixture prior model. No explicit computation of evidence was used. The dashed lines indicate the location of the boundaries from a buried valley interpreted prior to this study.

terior realizations by construction, automatically avoiding the burn-in periods and correlation analysis required by Metropolis-based methods. The tradeoff is that the number of accepted models is not known beforehand, though accepted models are guaranteed to occur in proportion to the posterior probability density function.

5.2. Ensuring robust statistics with finite lookup tables

When using finite lookup tables, the rejection sampler may accept only a few (or even a single) model realization with sparse sampling, making posterior statistics unreliable. The annealing temperature addresses this practical limitation by broadening the acceptance probability, allowing more models to be selected from the lookup table. Increasing T

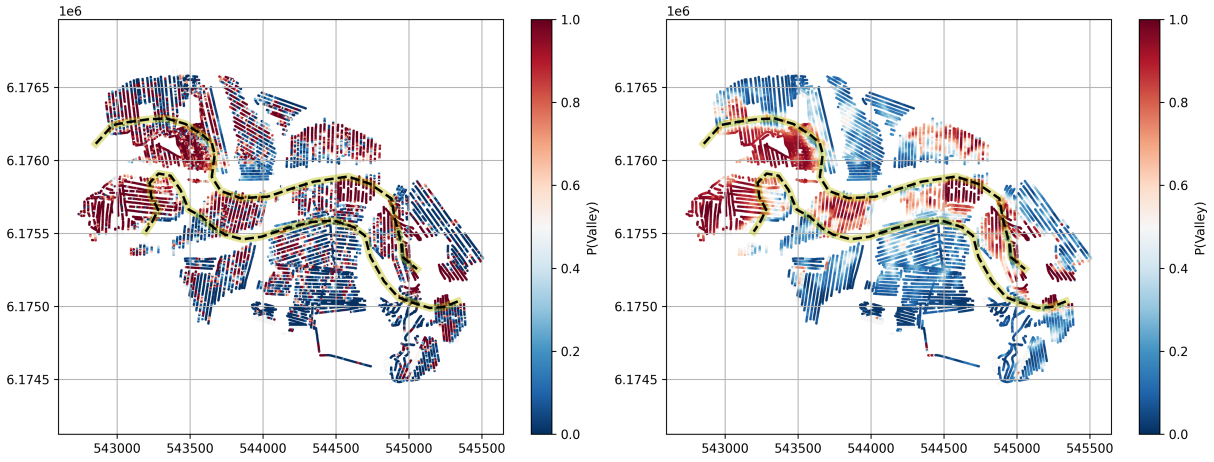

(a) $\sigma(H_{inside})$ using N=2×10^6

(b) $\sigma(H_{inside})$ using N=2×10^6, and noise inflated by a factor of 4.

Figure 11: Comparison of $\sigma(H_{inside})$ using different noise levels, obtained from the estimate of the evidence obtained inverting each hypothesis separately.

enables useful approximate posterior statistics to be computed even when the lookup table is too small to fully resolve the full posterior distribution.

5.3. Implications of noise model assumptions in EM inversion

Beyond enabling practical use of finite lookup tables, the annealing temperature also provides benefits for handling noise model discrepancies. Standard practice in electromagnetic inversion, as applied in the case study, assumes 3% uncorrelated Gaussian noise. However, observed data characteristics at moderate-to-high signal levels suggest that variability arises primarily from correlated effects, such as system drift or 3D modeling errors documented to exceed 3% with spatial correlation (Bai et al., 2021; Falk et al., 2025a; Heagy et al., 2025). When the assumed noise level underestimates true data uncertainty, the inversion attempts to fit residuals that exceed the assumed noise magnitude. This leads to overfitting, which degrades results for any inversion method. For probabilistic inversions specifically, underestimated noise causes the likelihood function to become artificially narrow, resulting in posterior distributions that are unrealistically concentrated and fail to reflect true parameter uncertainty, and that in addition will be computationally hard to sample.

Within INTEGRATE, automatic annealing temperature selection mitigates this issue by broadening the likelihood function while adapting locally to observed data quality. An annealing temperature greater than one effectively increases the noise level in the likelihood calculation, compensating for underestimated noise assumptions and reducing the influence of model-data mismatches such as those caused by unmodeled 3D effects. Both automatic annealing and appropriately increased noise levels prevent the inversion from overfitting to residuals, yielding more reliable posterior distributions. Support for both uncorrelated and correlated Gaussian noise models provides a foundation for future extensions to explicitly account for structured noise, which may improve stability when inverting data affected by complex 3D effects.

5.4. Hypothesis testing and model comparison

Hypothesis testing within INTEGRATE extends beyond the geological scenarios demonstrated here. Any modeling choice (prior model selection, noise assumptions, or forward modeling strategy) can be formulated as a hypothesis and evaluated via evidence-based comparison using Eq. 12.

5.5. Computational efficiency

The extended rejection sampler applied to 1D EM inversion is highly efficient, with performance depending mainly on lookup table size, number of soundings, and forward model complexity. Multiprocessing is implemented for both forward modeling (using the GA-AEM code (Brodie, 2020)) and posterior sampling. Figure 12 shows scaling across different processor counts ($N_{\text{proc}} = [1, 2, 4, 8, 16, 24]$) and lookup table sizes ($N = [10^4 - 10^6]$). Using a Linux workstation with 96GB RAM and an Intel Core 13900KF processor (8 performance cores and 16 efficiency cores). Forward computations scale almost perfectly across the 8 performance cores, while the memory-intensive rejection sampler suggest that no more than 8 cores should be used due to memory bandwidth constraints.

For the Daugaard data set (11,693 soundings), even with $N = 10^6$, the total CPU time per sounding is only a few seconds, which is over 200 times faster than comparable Metropolis-based implementations (Hansen and Minsley, 2019; Foks and Minsley, 2020). In contrast, Ray et al. (2024) required 41,600 cores for 2.8 hours to invert 242,742 soundings (equivalent to 30 CPU minutes per sounding), whereas the extended rejection sampler requires only about 2 seconds per sounding on a single CPU, leading to roughly 5.5 days on one CPU, or less than a day on a standard multicore workstation, for the full survey. Keep in mind, the results presented above, e.g. Figs 7-8, suggest that useful posterior statistics

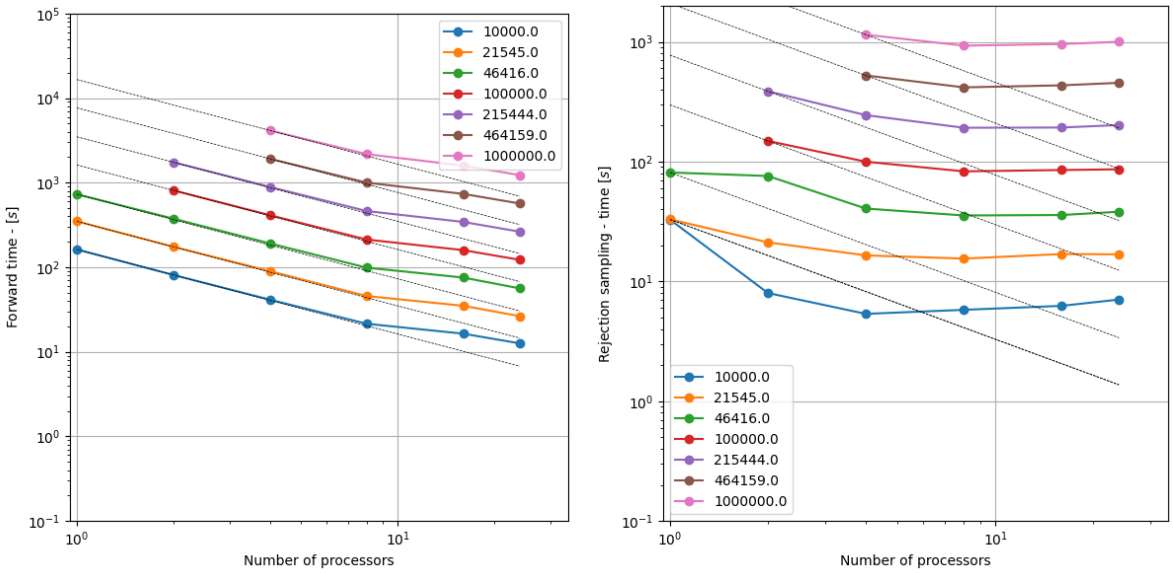

Figure 12: Timings for left) computing forward data using ga-aem, and right) rejection sampling tTEM data using the extended rejection sampler, for differents number of CPUs used, amd different sizes of the lookup table, N. Computation times were performed on a Linux server 96 GB RAM, and in intel 13900KF CPU.

may be obtained using a significantly smaller lookup table size, further reducing the computation time by a factor of 10, using for example $N = 10^5$ instead of $N = 10^6$.

Figure 13a shows the fraction of total computation time, used by 1) sampling the prior, 2) computing forward data, 3), performing rejection sampling, and 4) computing posterior statistics, for the Daugaard data set. For realistic sized lookup tables ($N > 10^5$) almost all computation time is split between forward computation and rejection sampling. Figure 13b shows the corresponding total computation time, using different numbers of cores and different lookup tables.

Importantly, these inversions require no access to high-performance computing facilities, enabling practitioners to perform full probabilistic inversions on ordinary desktop systems and support exploratory analysis, all essential steps towards broader adoption of probabilistic inversion in practice.

5.6. Limitations

The main limitation of the current application of the extended rejection sampler is that all results are inherently one-dimensional. Approaches such as those by Auken and Christiansen (2004); Viezzoli et al. (2008) incorporate spatial correlation between soundings to derive quasi-2D or 3D models. In contrast, we advocate imposing spatial constraints only after inversion to avoid introducing potentially incorrect dependencies during the inversion itself. Such post-inversion spatial integration can be achieved using a range of established geostatistical simulation and estimation techniques (Deutsch and Journel, 1992; Goovaerts, 1997; Marietoz and Caers, 2014).

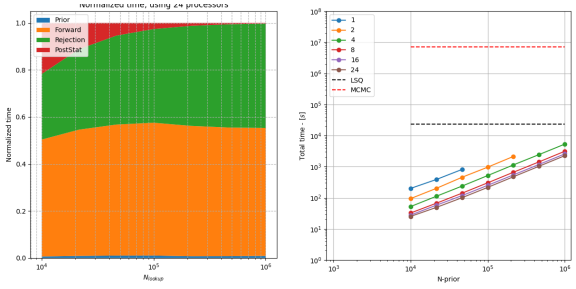

Figure 13: Left) The ratio of the total computation time for 1) sampling the prior, 2) computing prior data, 3) running the rejection sampler, and 4) computing statistics of the posterior. Right) Total computation time per sounding for the Daugaard data set, using different sizes of the lookup table, N, and different number of processors, $Nproc$. The dashed black line indicates the expected inversion time using laterally constrained inversion (Auken and Christiansen, 2004; Viezzoli et al., 2008) and the red dashed line the expected CPU time needed by using the extended Metropolis algorithm (Hansen et al., 2016).

6. Conclusions

The INTEGRATE Python package provides a computationally efficient framework for probabilistic inversion of localized geophysical data, particularly electromagnetic measurements. By implementing an extended rejection sampler with lookup tables, it achieves speedups exceeding 200× compared to traditional MCMC approaches while allowing the use of arbitrarily complex prior information involving both continuous and discrete model parameters.

A key strength of the framework is its ability to integrate detailed geological knowledge through flexible prior mod-

els that jointly describe continuous variables (e.g., resistivity with non-Gaussian distributions) and discrete categorical properties (e.g., lithological classes). This overcomes a fundamental limitation of conventional deterministic approaches, which typically rely on simple Gaussian priors and cannot readily incorporate heterogeneous geological information from maps, boreholes, or expert interpretation.

The framework further enhances practical applicability through automatic annealing temperature selection that ensures robust posterior statistics across varying data conditions, and through efficient evidence computation that enables formal hypothesis testing and Bayesian model comparison. Support for both continuous and discrete data is achieved through multivariate Gaussian and multinomial noise models, while the overall computational efficiency remains sufficient to run full probabilistic inversions on standard desktop hardware.

The Daugaard case study illustrates the framework's capability to integrate complex geological hypotheses through mixed prior models, successfully inverting 11,693 tTEM soundings while providing full uncertainty quantification. INTEGRATE thus represents a practical step forward in making probabilistic inversion accessible for routine use, removing the computational and modeling barriers that have long limited its application in geophysical practice.

7. Acknowledgments

This work is part of the INTEGRATE project (Hansen and Gulbrandsen, 2024) funded by Innovation Fund Denmark, Grant #2081-00009B.

Code availability section

```
Name of the code/library: INTEGRATE
Contact: tmeha@geo.au.dk
Hardware requirements: Any computer that can run Python 3.11 or later.
Program language: Python 3.11 or later.
Software required: Python
Program size: ...
The source codes are available for downloading at the link:
https://github.com/cultpenguin/integrate_module

License: MIT
```

Declaration of generative AI in writing During the preparation of this work, the authors used Claude (Anthropic) and ChatGPT (OpenAI) to improve clarity and readability of text, and Github CoPilot and Claude as coding assistants. After using this tool, the authors reviewed and edited the content as needed and take full responsibility for the content of this publication.

Declaration of competing interest The authors have no known competing financial interests or personal relationships that could have appeared to influence the work reported in this paper.

References

Amaya, M., Linde, N., Laloy, E., 2021. Adaptive sequential monte carlo for posterior inference and model selection among complex geological priors. Geophysical Journal International 226, 1220–1238.

Auken, E., Christiansen, A.V., 2004. Layered and laterally constrained 2d inversion of resistivity data. Geophysics 69, 752–761.

Auken, E., Christiansen, A.V., Jacobsen, B.H., Foged, N., Sørensen, K.I., 2005. Piecewise 1d laterally constrained inversion of resistivity data. Geophysical Prospecting 53, 497–506.

Auken, E., Foged, N., Larsen, J.J., Lassen, K.V.T., Maurya, P.K., Dath, S.M., Eiskjær, T.T., 2019. ttem - a towed transient electromagnetic system for detailed 3d imaging of the top 70 m of the subsurface. Geophysics 84, E13–E22. doi:10.1190/geo2018-0355.1.

Auken, E., Viezzoli, A., Vest Christiansen, A., 2009. A single software for processing, inversion, and presentation of aem data of different systems: The aarhus workbench. ASEG Extended Abstracts 2009, 1–5.

Bai, P., Vignoli, G., Hansen, T.M., 2021. 1D stochastic inversion of airborne time-domain electromagnetic data with realistic prior and accounting for the forward modeling error. Remote Sensing 13, 3881.

Barfod, A., Møller, I., Christiansen, A., 2016. Compiling a national resistivity atlas of denmark based on airborne and ground-based transient electromagnetic data. Journal of Applied Geophysics doi:10.1016/j.jappgeo.2016.09.017.

Brodie, R.C., 2020. GA-AEM - Geoscience Australia airborne electromagnetics programs. https://github.com/GeoscienceAustralia/ga-aem.

Cordua, K.S., Hansen, T.M., Mosegaard, K., 2012. Monte carlo full-waveform inversion of crosshole gpr data using multiple-point geostatistical a priori information. Geophysics 77, H19–H31.

Deutsch, C.V., Journel, A.G., 1992. GSLIB: Geostatistical Software Library and User's Guide. Oxford University Press.

Falk, F., Vest, A.V., Hansen, T.M., 2025a. Quantifying 3D modeling errors in time-domain electromagnetics: Implications for deterministic and probabilistic inversions. Geophysics Submitted, In review.

Falk, F.A., Christiansen, A.V., Hansen, T.M., 2025b. Comparison of three one-dimensional time-domain electromagnetic forward algorithms. Applied Computing and Geosciences , 100243doi:10.1016/j.acags.2025.100243.

Foks, N., Minsley, B., 2020. Geophysical Bayesian inference in Python (GeoBiPy). https://github.com/usgs/geobipy. doi:10.5066/P9K3YH9O.

Golub, G.H., Hansen, P.C., O'Leary, D.P., 1999. Tikhonov regularization and total least squares. SIAM journal on matrix analysis and applications 21, 185–194.

Goovaerts, P., 1997. Geostatistics for Natural Resources Evaluation. Applied Geostatistics, Oxford University Press.

Hansen, T.M., 2021. Efficient probabilistic inversion using the rejection sampler—exemplified on airborne EM data. Geophysical Journal International 224, 543–557. doi:10.1093/gji/ggaa491.

Hansen, T.M., Cordua, K.C., Mosegaard, K., 2012. Inverse problems with non-trivial priors - efficient solution through sequential Gibbs sampling. Computational Geosciences 16, 593–611. doi:10.1007/s10596-011-9271-1.

Hansen, T.M., Cordua, K.S., Looms, M.C., Mosegaard, K., 2013. SIPPI: a Matlab toolbox for sampling the solution to inverse problems with complex prior information: Part 1, methodology. Computers & Geosciences 52, 470–480. doi:10.1016/j.cageo.2012.09.004.

Hansen, T.M., Cordua, K.S., Zunino, A., Mosegaard, K., 2016. Probabilitsic Integration of Geo-Information, in: Moorekamp, M. (Ed.), Joint Inversion. John Wiley & Sons. volume 218, pp. 93–116.

Hansen, T.M., Gulbrandsen, M.L., 2024. Informative mapping of construction aggregate resources through statistical data analysis (INTEGRATE), in: GEOSTATS 2024. chapter 30, pp. 367–382.

Hansen, T.M., Minsley, B.J., 2019. Inversion of airborne EM data with an explicit choice of prior model. Geophysical Journal International 218, 1348–1366. doi:10.1093/gji/ggz230.

Hansen, T.M., Mosegaard, K., Cordua, K.C., 2008. Using geostatistics to describe complex a priori information for inverse problems, in: Ortiz, J.M., Emery, X. (Eds.), VIII International Geostatistics Congress, Mining Engineering Department, University of Chile. pp. 329–338.

Heagy, L.J., Oldenburg, D.W., Kang, S., Yang, D., 2025. Why every electromagnetic inversion needs a 3d forward simulation. The Leading Edge 44, 847–854. doi:10.1190/tle44110847.1.

Jørgensen, F., Møller, R.R., Sandersen, P.B., Nebel, L., 2010. 3-d geological modelling of the egebjerg area, denmark, based on hydrogeophysical data. Geological Survey of Denmark and Greenland Bulletin 20, 27–30.

Laloy, E., Vrugt, J.A., 2012. High-dimensional posterior exploration of hydrologic models using multiple-try dream (zs) and high-performance computing. Water Resources Research 48.

Linde, N., Renard, P., Mukerji, T., Caers, J., 2015. Geological realism in hydrogeological and geophysical inverse modeling: A review. Advances in Water Resources 86, 86–101.

MacKay, D.J., 1992. Bayesian interpolation. Neural computation 4, 415–447.

Madsen, R.B., Høyer, A.S., Sandersen, P.B., Møller, I., Hansen, T.M., 2023. A method to construct statistical prior models of geology for probabilistic inversion of geophysical data. Engineering Geology 324, 107252.

Mariethoz, P., Caers, P., 2014. Multiple-point Geostatistics: Stochastic Modeling with Training Images. Wiley. URL: https://books.google.dk/books?id=kQX2oAEACAAJ.

Menke, W., 2012. Geophysical data analysis: Discrete inverse theory. volume 45. Academic Press.

Metropolis, N., Rosenbluth, M., Rosenbluth, A., Teller, A., Teller, E., 1953. Equation of state calculations by fast computing machines. J. Chem. Phys. 21, 1087–1092.

Minsley, B.J., 2011. A trans-dimensional Bayesian Markov chain Monte Carlo algorithm for model assessment using frequency-domain electromagnetic data. Geophysical Journal International 187, 252–272.

Mosegaard, K., Tarantola, A., 1995. Monte Carlo sampling of solutions to inverse problems. J. geophys. Res 100, 12431–12447.

Mosegaard, K., Tarantola, A., 2002. Probabilistic approach to inverse problems, in: Lee, W., Kanamori, H., Jennings, P., Kisslinger, C. (Eds.), International handbook of earthquake and engineering seismology. WHK Lee et al. volume 81A. chapter 16, pp. 237–265.

Neal, R.M., et al., 2011. Mcmc using hamiltonian dynamics. Handbook of markov chain monte carlo 2, 2.

Nørgaard, J., Madsen, R.B., Høyer, A.S., Møller, I., Hansen, T.M., 2026. GeoPrior1D: An application for generating 1D geological and geophysical realizations of the subsurface. SoftwareX Submitted, In review.

Ray, A., Douglas, A., van der Wielen, S., Ley-Cooper, Y., Brodie, R.C., Symington, N., Nicoll, M., Wong, S., Sun, Y., Czarnota, K., 2024. Probabilistic airborne electromagnetic (AEM) inversion of 20-km AusAEM data: Phase 1. Technical Report. Geoscience Australia. Canberra. doi:10.26186/149375. eCat ID 149375.

Sambridge, M., 1999. Geophysical inversion with a neighbourhood algorithm—i. searching a parameter space. Geophysical journal international 138, 479–494.

Sambridge, M., Gallagher, K., Jackson, A., Rickwood, P., 2006. Trans-dimensional inverse problems, model comparison and the evidence. Geophysical Journal International 167, 528–542.

Sambridge, M., Mosegaard, K., 2002. Monte carlo methods in geophysical inverse problems. Reviews of Geophysics 40, 3–1.

Sivia, D., Skilling, J., 2006. Data analysis: a Bayesian tutorial. OUP Oxford.

Spremić, M., Eidsvik, J., Hansen, T.M., 2025. Local conditioning in posterior sampling methods with example cases in subsurface inversion. Computers & Geosciences , 105863.

Strebelle, S., 2002. Conditional simulation of complex geological structures using multiple-point statistics. Mathematical Geology 34, 1–21.

Tarantola, A., 2005. Inverse problem theory and methods for model parameter estimation. SIAM.

Tarantola, A., Valette, B., 1982a. Generalized nonlinear inverse problems solved using the least squares criterion. Rev. Geophys. Space Phys 20, 219–232.

Tarantola, A., Valette, B., 1982b. Inverse problems= quest for information. J. Geophys 50, 150–170.

Viezzoli, A., Christiansen, A.V., Auken, E., Sørensen, K., 2008. Quasi-3D modeling of airborne TEM data by spatially constrained inversion. Geophysics 73, F105–F113.

Zunino, A., Gebraad, L., Ghirotto, A., Fichtner, A., 2023. HMCLab: a framework for solving diverse geophysical inverse problems using the Hamiltonian Monte Carlo method. Geophysical Journal International 235, 2979–2991.

Appendix

A. Prior from Daugaard

Figures A01-A03 show 100 realizations of $\rho_{inside}(\mathbf{m},\mathbf{n})$, $\rho_{outside}(\mathbf{m},\mathbf{n})$, and $\rho_{mixture}(\mathbf{m},\mathbf{n})$, as well as the corresponding 1D marginal distributions.

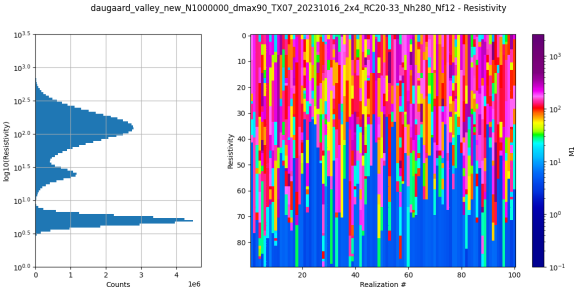

(a) 1D marginal distributions of resistivity $\rho_{inside}(\mathbf{m})$ (left) and 100 realizations of $\rho_{inside}(\mathbf{m})$ (right).

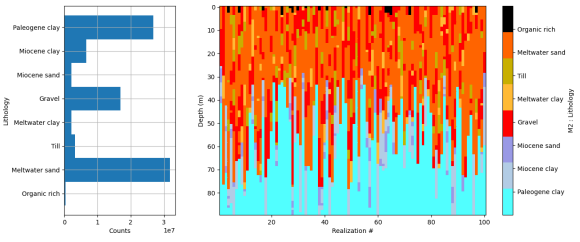

(b) Marginal distributions of lithology $\rho_{inside}(\mathbf{n})$ (left) and 100 realizations of $\rho_{inside}(\mathbf{n})$ (right).

Figure A01: Summary statistics for $\rho_{inside}(\mathbf{m},\mathbf{n})$.

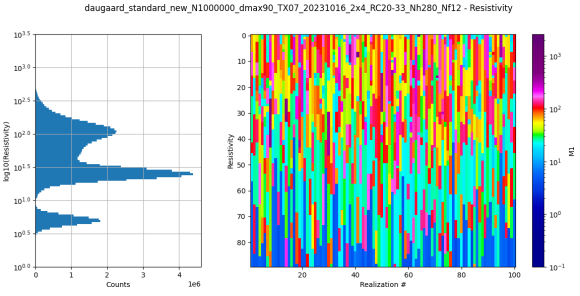

(a) 1D marginal distributions and 100 realizations of resistivity $\rho_{outside}(\mathbf{m})$.

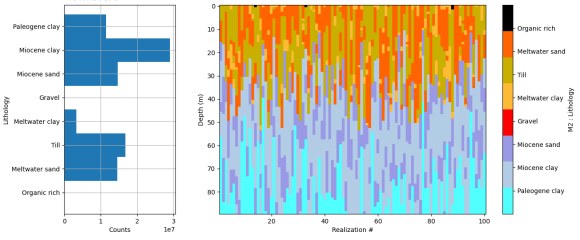

(b) Marginal distributions and 100 realizations of lithology $\rho_{outside}(\mathbf{n})$.

Figure A02: Summary statistics for $\rho_{outside}(\mathbf{m},\mathbf{n})$.

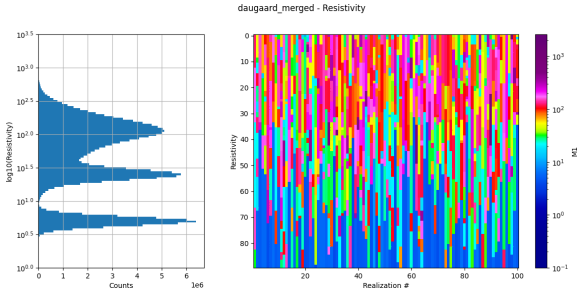

(a) 1D marginal distributions of resistivity $\rho_{mixture}(\mathbf{m})$.

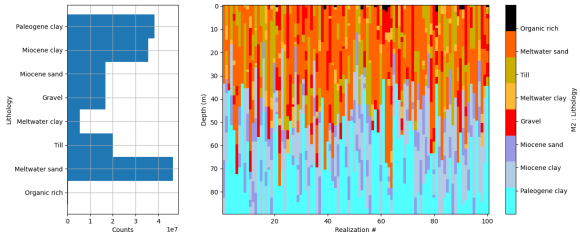

(b) Marginal distributions of lithology $\rho_{mixture}(\mathbf{n})$.

Figure A03: Summary marginal statistics for $\rho_{mixture}(\mathbf{m},\mathbf{n})$.